CHAPTER IV

RESULTS AND DISCUSSION

4.1. Synthesis of coral-liked gold nanostructures

The color of silver globule rapidly changed from silver to dark blue within 30 min indicating a progress of galvanic reaction when an ultrasonic-cleaned silver globule was immersed into a 5,000 ppm of Au^{3+} solution. The orange-yellow color of the gold (III) ion solution was insignificantly changed although the color of silver globule was completely altered. An insignificant change in the UV/visible spectra was also observed. Figure 4.1 shows UV–visible absorption spectra of aqueous Au^{3+} solution before and after galvanic replacement reaction. The spectrum revealed a strong absorption band at 220 nm and a shoulder at 290 nm of Au^{3+} solution before galvanic replacement reaction, These bands were assigned as ligand-to-metal-charge-transfer (LMCT) transitions [61, 62]. The phenomenon indicates that the replacement reaction only occurs at the surface while minute amount of gold (III) ion was consumed by the reaction. The UV/visible spectra were dominated by the unreacted gold (III) ion complex showing that there was no silver ion (Ag^+) releasing into the solution. After prolong reaction time of 30 min, the solution was still clear while the UV/visible spectrum showed an undetectable change. These phenomena indicated that the galvanic generated AgCl was firmly attached on the surface of silver globules releasing of Ag^+ into the solution. AgCl was not released into the solution since there was no observable baseline shift after a prolong reaction time. The solution was still clear indicating that the galvanic-generated AgCl was attached no silver surface.

SEM micrographs of the galvanized silver globules (Figure 4.2) were in good agreement with the color change as the smooth surface of the silver globules was extensively damaged. A rougher surface could be noticed even from a low magnification image.

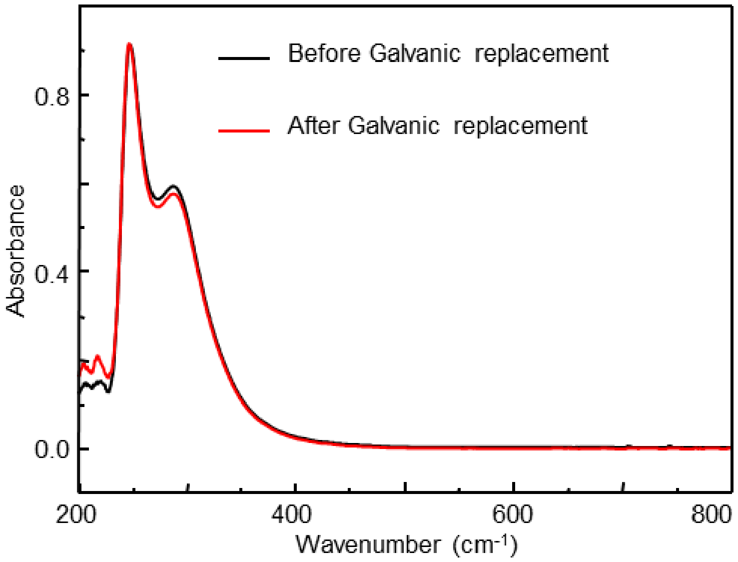

Figure 4.1 UV-visible spectra of 5,000 ppm Au^{3+} diluted to 10 ppm non reaction and 30 min galvanic replacement reaction.

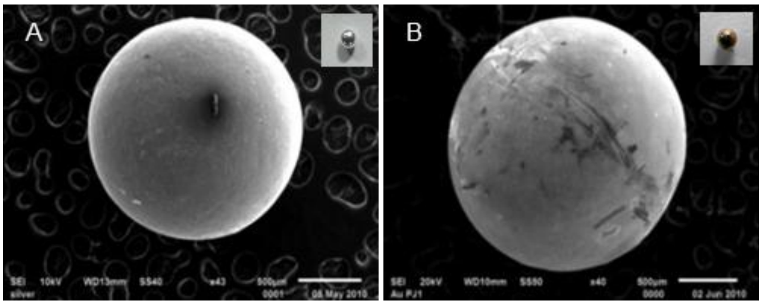

Figure 4.2 (A, B) Low magnification SEM micrographs of silver globules observed before and after galvanic replacement reaction 30 min, (inset) digital image of silver globules.

The elemental composition after 30 min galvanic replacement reaction was investigated by energy dispersive X-ray spectroscopy (EDS). Figure 4.3A EDS spectrum displayed strong peaks at 2.21, 2.62, and 2.98 keV which corresponding to Au, Ag, and Cl character. By following the ZAF method, the calculated elemental composition of Au/Ag/Cl ratio was about 14.67, 67.35, and 17.97 % atom. These results implied that galvanic replacement reaction generated solid AgCl formation co-deposited with Au atom [53]. The EDS spectrum (Figure 4.3B) shows high intensity of Au and low intensity of Ag such that, 94.32 and 5.86 % atom after removing the AgCl solid with a NH_3 solution (ammonia treatment), while the signal for Cl was not detected. From the EDS data, it could be explained that the galvanic replacement reaction generated Au/AgCl composites and changed to pure Au structures after ammonia treatment. SEM micrographs (Figure 4.3A inset) showed the smooth morphology of AgCl patches with domain size of 1-2 µm covered with gold structures. Selectively dissolution of AgCl patches was performed by 10 % w/v NH_3 solution. Missing the large morphology of AgCl and the porosity of CLGNs with high surface roughness was appeared when AgCl was removed. The morphology of gold nanostructures is similar to a coral which called coral-liked gold nanostructures.

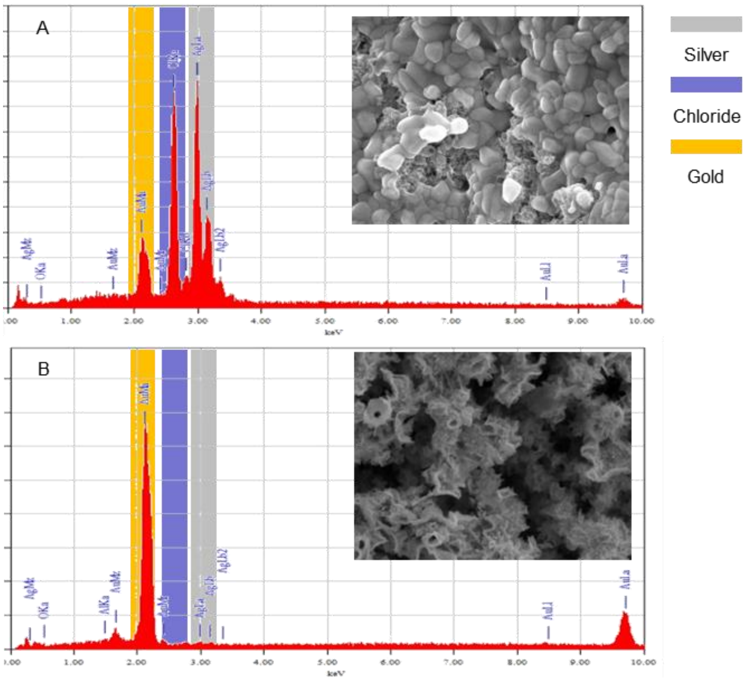

Figure 4.3 (A, B) Energy dispersive X-ray spectra of Au/AgCl layer with 30 min. before and after ammonia treatment, (inset) SEM micrographs of corresponding condition.

To confirm galvanic generated Au/AgCl composites by EDS mapping, the elemental distribution was displayed in Figure 4.4 showing Au, Ag, and Cl contents of Au/AgCl composites and CLGNs. Black and pink areas indicated low and high signal of those elements. The pink areas of Ag and Cl maps (Figure 4.4 A3, A4) are more than that of Au map (Figure 4.4 A2) before AgCl removing. On the other hand, larger pink area of gold maps (Figure 4.4 B2) comparing with Ag and Cl was observed after AgCl removing.

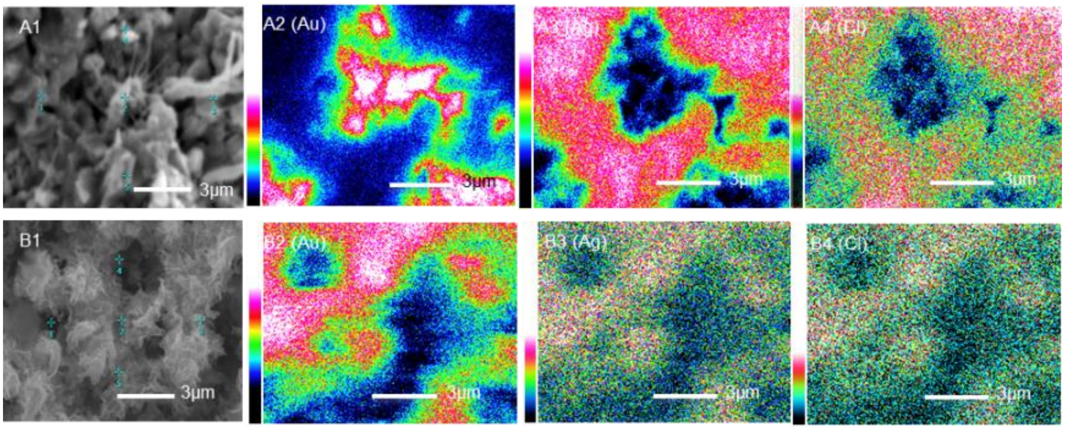

Figure 4.4 Elemental distributions at 30 min galvanic replacement reaction of silver globules and 5,000 ppm of Au^{3+}. (A1) SEM micrographs of galvanized silver globule surface before ammonia treatment, (A2-A4) Au, Ag, and Cl maps before ammonia treatment of silver surface. (B1-B4) corresponding SEM micrograph and EDS maps after remove AgCl by ammonia treatment.

The galvanic replacement reaction is one of the simple methods for creating complex structures (e.g., thin film, hollow structure, porous structure, bi metallic, and alloy) by consuming the more sacrificed metal component [63, 64]. When immersing silver metal into gold (III) ion solution, silver metal which acted as anode site was rapidly oxidized resulting Ag^+ and electrons (equation (5)). The electrons transfer to surface that acted as cathode site which captured Au^{3+} on silver surface generating Au^0 and Cl^- (equation (6)), while Cl^- reacted with Ag^+ and became AgCl (equation (7)). The solubility product (K_{sp}) of AgCl in water about 1.8×10^{-10} at 20°C due to solid AgCl co-deposited with gold [53, 65]. The size of AgCl patches is bigger than Au that controls Au deposition through AgCl layer, according to stoichiometry of AgCl which is 3 times more than Au. However, galvanic replacement reaction generated excess Cl^- into environmental reaction. The solubility of AgCl was decreased in the atmosphere of the excess Cl^- environment due to the common ion effect as shown in equation (8) [65-67]. However ammonia treatment method was as a tool for studying the influential CLGNs formation as shown in Figure 4.6 as well as equation (9).

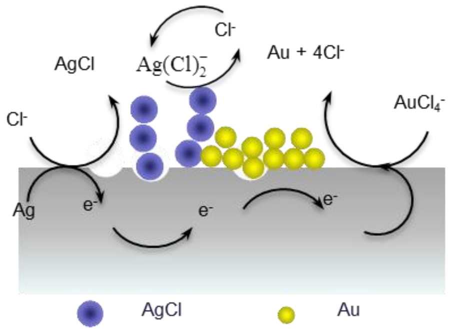

$$Ag(s) \rightarrow Ag^+(aq)+e^- \quad (5)$$

$$AuCl_4^-(aq)+e^- \rightarrow Au(s)+4Cl^-(aq) \quad (6)$$

$$3Ag(s)+Au(s)+3AgCl(s)+Cl^-(aq) \quad (7)$$

$$AgCl(s)+Cl^-(aq) \leftrightarrow Ag(Cl)_2^-(aq) \quad (8)$$

Figure 4.5 Schematic diagram of galvanic replacement reaction shows Au/AgCl co-depositions on sacrificed silver surface, *i.e.*, as the film become thicker. Equation (5, 6) oxidation and reduction reaction occurred as anode and cathode site. Equation (7) shows total galvanic replacement reaction. Common ion effects of AgCl are also depicted in equation (8).

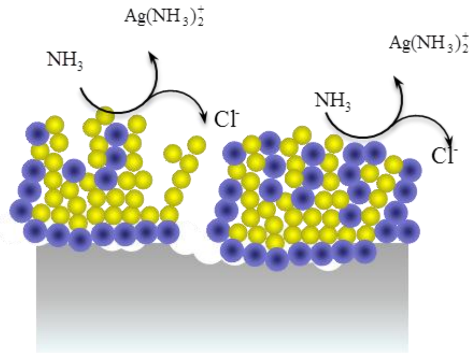

$$AgCl(s)+2NH_3(aq) \leftrightarrow Ag(NH_3)_2^+(aq)+Cl^-(aq) \quad (9)$$

Figure 4.6 AgCl dissolution process by ammonia treatment (NH_3).

4.1.1. The concentration effect of Au^{3+}solutions on gold structures

Optical property of galvanized silver surface changes when increasing the concentration of Au^{3+}. Figures 4.7(A, B) show digital images of Au^{3+} solution at various concentrations (0, 50, 100, 500, 1,000, and 5,000 ppm) before immersing and immersing silver globules at 30 min of galvanic replacement reaction. At low concentrations, 50 and 100 ppm Au^{3+}, the yellow color did not appear while the light yellow was noticed at 500 ppm. The optical property of silver surface significantly changes when immersing silver globule at various Au^{3+} concentrations. At 50 and 100 ppm, the optical property of galvanized silver surface was not clearly changed. The galvanic reaction of low Au^{3+}concentrations and silver sacrificed layer was not change optical property of silver surface. Ultrathin film gold with 5nm was continuously deposited on substrate showing highly transparent property of gold film [68]. Light brown was appeared when increased concentration of Au^{3+} up to 500 ppm. The silver surface color was changed to black at high concentration, 1,000 and 5,000 ppm. Light brown and black result from the thinness of Au/AgCl composites was increased due to galvanic replacement reaction.

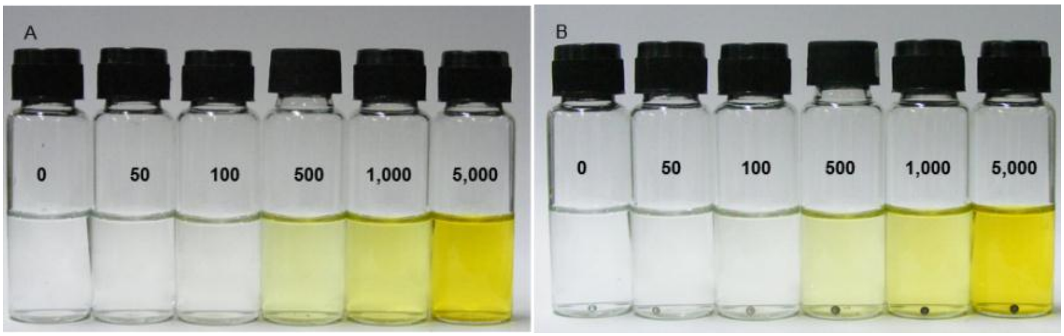

Figure 4.7 (A) Digital images of Au^{3+} concentration at 0, 50, 100, 500, 1,000, and 5,000 ppm. (B) Corresponding condition (A) of silver globule after 30 min of galvanic replacement reaction.

SEM micrographs were used to follow the structural evolution involving as various Au^{3+} concentrations. As the concentration of Au^{3+} increased from 50 ppm to 5,000 ppm, more complex Au structures were observed. At low concentration of Au^{3+} (Figure 4.8 A2, 50 ppm), spherical AgCl precipitated with domain size of 0.1-0.3 µm and scattered over the surface and aggregated to clusters

AgCl with domain size of 1.0-3.0 µm and were generated over the surface of silver surface. The clusters of AgCl precipitates grew larger once Au^{3+} was increased to 100 ppm (Figure 4.8 A3, 100 ppm). When the concentration of Au^{3+} was increased to 500 ppm (Figure 4.8 A4, 500 ppm), a plate-liked AgCl precipitates of smaller domain (1 µm) were generated. An even smaller plate-liked silver precipitation was obtained as the concentration of Au^{3+} was increased to 1,000 ppm (Figure 4.8 A5, 1,000 ppm). However, as the concentration of Au^{3+} was increased to 5,000 ppm (Figure 4.8 A6), larger plate-liked AgCl precipitations with smooth surface were obtained. The evidence of gold structures was observed in this condition by removing AgCl. After the removal of AgCl precipitates by ammonia treatment, the gold nanostructures were revealed. At low concentration of Au^{3+} (Figure 4.8 B2, 50 ppm), spherical gold nanoparticles with particle size of 80-400 nm were developed. Gold structures with plate-liked nanostructures start developing at 100 ppm of Au^{3+} concentration (Figure 4.8 B3). As the concentration of Au^{3+} increased (Figure 4.8 B4, 500 ppm), the gold plate with thickness size of 40-60 nm was grown in the direction normal to the silver surface. The plate length was increased when increasing concentration of Au^{3+} to 1,000 ppm (Figure 4.8 A5). As the concentration of Au^{3+} increased, larger and more delicate CLGNs were developed. The delicate CLGNs observed in Fig. 4.8 B6 suggest that the AgCl precipitates, which concomitantly generated with the gold structures, that prevented the collapse of the gold structures as the CLGNs grew inside the AgCl precipitates. Reaction rate of galvanic replacement depended on the concentrations of Au^{3+} [65]. The effect of Au^{3+} concentration on gold structures was confirmed by Nernst equation as shown in equation (6) [66]. Oxidation potential of galvanic replacement reaction depended on E_{cell} of reaction that related with concentration of Au^{3+}. Concentration of Au^{3+} was increased, deposition rate of Au atoms and AgCl were increased due to the oxidation potential of Au^{3+}. More complex gold structures were created with high concentration of Au^{3+} when prolonging reaction time.

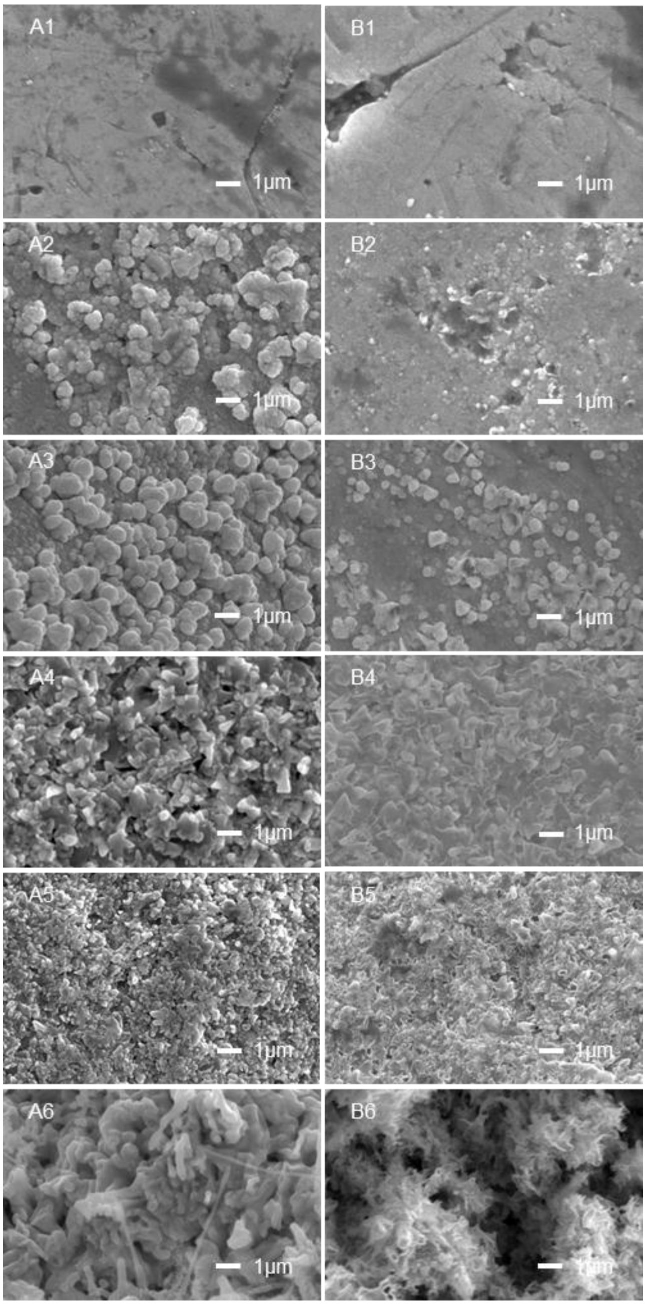

Figure 4.8 Structural developments of CLGNs due to concentration of Au^{3+} with 30 min reaction time. (A1-A6 and B1-B6) SEM micrographs of Au/AgCl composites and Au nanostructures increase the concentrations, 0, 50, 100, 500, 1,000, and 5,000 ppm Au^{3+} at 30 min of reaction time.

For an M^{m+}/M couple: $$E=E^0+\left(\frac{RT}{zF}\text{In}\left[M^{n+}\right]\right) \quad (6)$$

Where R = Molar gas constant = 8.314 $JK^{-1}mol^{-1}$

T = emperature in K

Z =Number of moles electrons transferred per mole of reaction

F = Faraday constant = 96485 $Cmol^{-1}$

Mn^+ = Au^{3+} concentration in mol dm^{-3}

Elemental composition on galvanized silver surface with 50, 100, 500, 1,000, and 5,000 ppm of Au^{3+} was explored as shown in Figure 4.9. The atomic ratio of Ag/Au before ammonia treatment will be decreased when the Au^{3+} concentration increased from 50 to 500 ppm as 45.8, 13.80, and 3.70. Conversely, atomic ratio of Ag/Au was slightly changed when increasing the concentration of Au^{3+} up to 5,000 ppm, about 3.4, and 2.3. The atomic ratios of Ag/Au after ammonia treatment with any Au^{3+} concentration was decreased comparable before ammonia treatment. On the other hand, atomic ratio of Cl/Au before ammonia treatment insignificantly changed when increased the concentration of Au^{3+} to 5,000 ppm. But atomic ratio of Cl/Au at each concentration after ammonia treatment was decreased. Penetration depth of electron interaction with matter can be calculated from Kanaya and Okayama mathematical model that it could be explained differently atomic ratio of Ag and Cl with Au. Penetration depth of electron interaction with Au film about 857.32 nm was calculated with 20 keV by following equation (7) [69].

$$R_{Au}(nm)=5.76E_0^{1.67} \quad (7)$$

Where R_{Au} = Bethe range, penetration depth (nm)

E_0 = Beam energy (keV)

If the thinness of galvanized layer is lower than 857.32 nm, the signal of silver sacrificed layer was observed at 20 keV. In our case, monitoring of transformative gold thinness was traced by atomic ratio of Ag/Au. The galvanic reaction of Ag and low concentration of Au^{3+} (50 and 100 ppm) atomic ratio of Ag/Au is higher than high concentration of Au^{3+} (500, 1,000, and 5,000 ppm). Since Ag content was measured from silver sacrifice layer and AgCl from galvanized-layer. Electrons can pass through galvanized-layer to silver sacrificed layer, due to the thinness of galvanized layer is lower than electron penetration depth. Since the thinness of galvanized layer at high concentration of Au^{3+} is higher than electron penetration depth, only Ag signal from galvanized layer was detected. Atomic ratio Ag/Au was decreased because electron cannot interact with silver sacrificed layer. However the atomic ratio of AgCl is more than the standard molar ratio of Ag/Cl. X-ray photoelectron spectroscopy (XPS) and EDS results, the molar ratio of Ag/Cl was about 1.05 and 1.03 but both XPS and EDS can easily decompose AgCl into Ag [70].

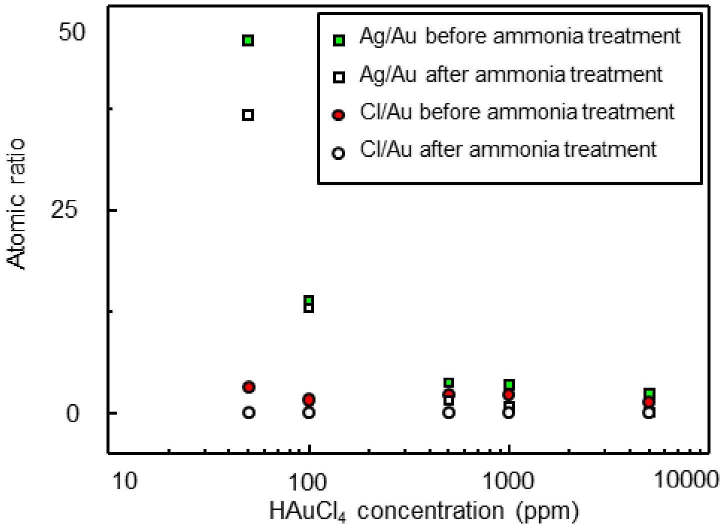

Figure 4.9 Elemental analysis of galvanized layer on silver surface with 0, 50, 100, 500, 1,000, and 5,000 ppm Au^{3+} solution at 30 min. (A) ratio of Ag/Cl (B, C) Au and Ag before and after ammonia treatment.

4.1.2. Time dependent evolution of CLGNs

Time dependent evolution of CLGNs at 5,000 ppm of Au^{3+} is followed by SEM. Figures 4.10 SEM micrographs of Au/AgCl and Au showed several morphology of gold nanostructure before and after ammonia treatment that can be monitored structural growth by following reaction time, 1, 5, 10, 20, and 30 min. As 1 min of reaction time (Figure 4.10 A1), spherical AgCl precipitates with domain size of 60-100 nm dispersed over the surface as well as aggregated to clusters AgCl with domain size of 1-3 µm were generated over the surface of silver. The clusters of AgCl precipitates grew larger as reaction time was increased to 5 min (Figure 4.10 A2). When the reaction time was greater than 10 min (Figure 4.10 A3), semi-continuing AgCl layer were generated. Continuing AgCl layer were obtained as the reaction time was increased to 20 min (Figure 4.10 A4). However, when the reaction time was increased to 30 min (Figure 4.10 A5), AgCl dissolution phenomenon was observed with generating the gap of AgCl. At the same condition, micro-channels with domain size of 0.5-1 µm of silver chloride layer were obviously detected. The micro-channels inside AgCl structures resulted with Cl^- envelopment, these channels through AgCl are the main path for ionic transport [47]. Finally, NLGNs start to grow through AgCl structures at 30 min galvanized time. An evidence of CLGNs was observed in this condition by removing AgCl. Porous gold film with pore size of 50-800 nm was developed at 1 min of galvanic replacement reaction as shown in Figure 4.10 B1. That porous gold was produced from selective dissolution of AgCl without gold structures. Gold nanostructures with plate-liked nanostructures start developing on gold film since 1 min and more plate-liked nanostructures when increasing galvanized time to 5 min (Figure 4.10 B2). As the reaction time of the galvanic replacement reaction was increased to 10 min (Figure 4.10 B3), the plate-liked gold nanostructures with thickness size of 40-60 nm grew at normal direction and increased porosity of structures. Similarly growing as CLGNs was developed at 20 min (Figure 4.10 B4). The complexity of CLGNs was increased when increasing galvanized time to 30 min (Figure 4.10 B5), while NLGNs start developing on plate-liked gold nanostructures at this condition. At 60 min of galvanic replacement reaction increased, a larger and more delicate CLGNs and NLGNs were developed. The delicate CLGNs observed in Figure 4.10 B6 suggested that the AgCl precipitate, which concomitantly generated with the gold structures, prevented the collapse of the gold nanostructures as the CLGNs grew inside the AgCl precipitates. Time dependent evolution of CLGNs development was confirmed by following the history of galvanized layer growth. The vertical panorama SEM micrograph was the new technique for characterization the detail of gold film layer. Figure 4.10 (C), cross section vertical panorama SEM micrograph with thinness 22 µm on CLGNs was captured at 30 min reaction time. The galvanized layer at initial state, dense gold was epitaxial depositing with layer thinness about 300 nm. The dense gold layer resulting epitaxial deposition of Au on silver surface was attached more than AgCl. This can be caused by the same lattice constants of gold (0.408) and silver (0.409), While the lattice constant of silver chloride (0.544) was different due to AgCl no epitaxial depositing on gold and silver [71]. The gold nanoporous clearly developed when the galvanized layer grew up to 500 nm. Gold nanoporous with 50-80 nm was observed at 500-5,000 ppm of Au^{3+} solution. Larger AgCl precipitate was formed as the thinness of galvanized layer increasing since 2 µm up to completely layer. That occurrence can be noticed from micro porous on CLGNs layer. The gain defect of AgCl and Au on Au/AgCl composites was appear due to different lattice constants.

4.1.3. AgCl under layer formation on the Au/AgCl composites

Figure 4.11 showed the SEM micrographs of CLGNs observed AgCl under layer formation phenomena. Cross-section of CLGNs at 5, 30, and 60 min before and after galvanic reaction were separated from Ag sacrificed surface. At 5 sec of galvanic replacement reaction, spherical gold with domain of 150-300 nm grew on sacrificed silver surface with thinness of 700-800 nm while the gain boundary of Ag indicated on the silver surface due to galvanic corrosion. After ammonia treatment the morphology and thinness of CLGNs is similar with that before ammonia treatment. The results confirmed epitaxial deposition of Au on silver surface and no epitaxial deposition of AgCl on Ag surface. Au atoms could be deposited on silver surface is more than AgCl, morphology of Au/AgCl nanocomposites after ammonia treatment was no observed. AgCl under layer formation was observed at 30 sec of galvanic reaction. The thinness of Au/AgCl composite before ammonia treatment about 1.6 µm was decreased to 1.2 µm after ammonia treatment. Then AgCl was detected on silver surface but porous structures on silver surface were noticed after ammonia treatment. The corrosive silver surface occurred while galvanic reaction was implied due to AgCl formation under layer. When prolonging the reaction, AgCl under layer was clearly generated between Au/AgCl composites and silver surface. The thinness of Au/AgCl composite and AgCl under layer about 2.6-3 µm before ammonia treatment was decreased to 1.9-2.3 µm after ammonia treatment.

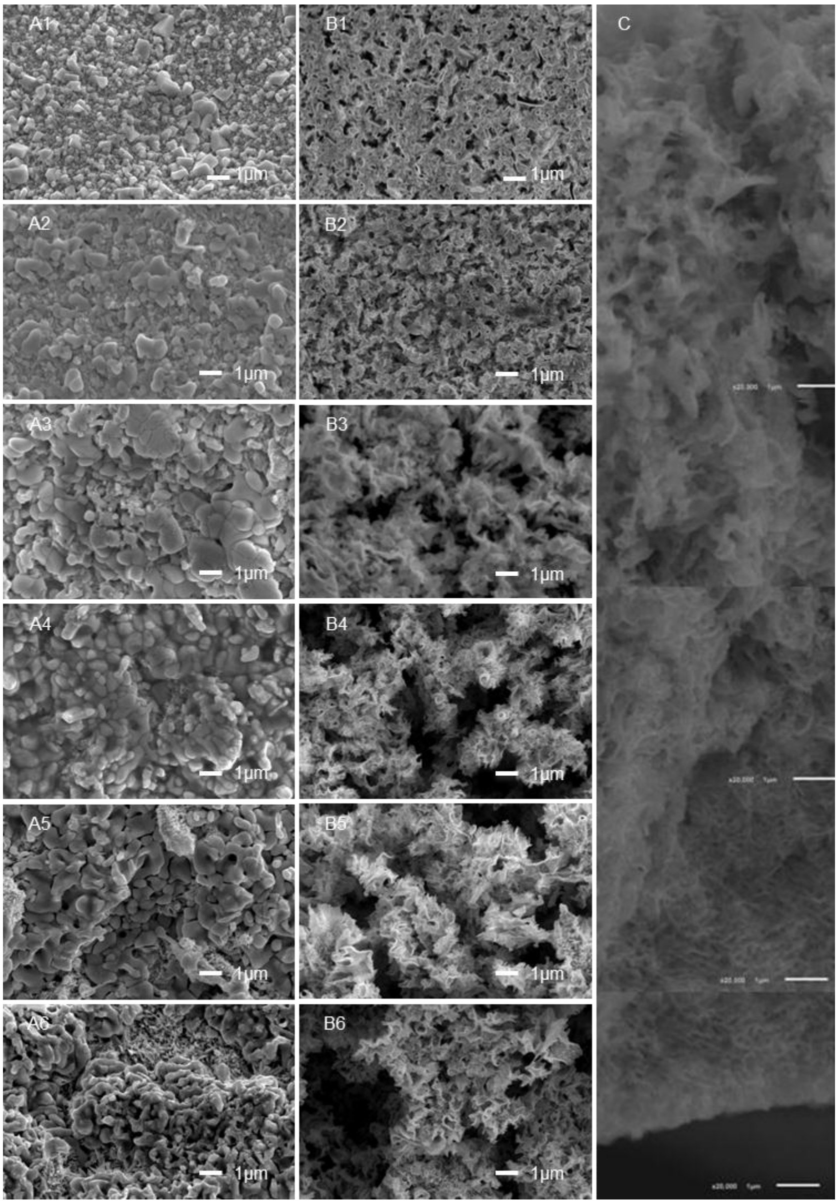

Figure 4.10 (A1-A6) Time dependent evolution of Au/AgCl co-deposited on silver globules surface by galvanic replacement reaction, silver globules and 5,000 ppm Au^{3+} at 1, 5, 10, 20, 30, and 60 min respectively, (B2-B6) structural development of gold after removing silver chloride by ammonia treatment. (C) Cross section vertical panorama SEM micrograph on CLGNs with 30 min reaction time.

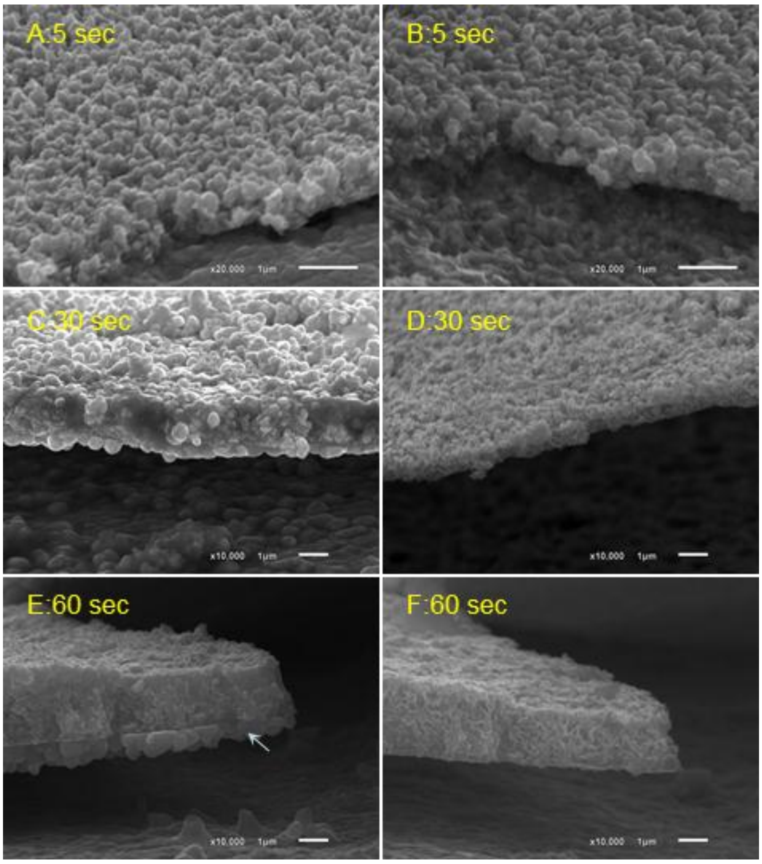

Figure 4.11 (A, C, and E) SEM micrographs of cross section galvanized silver surface with 5,000 ppm Au^{3+} at 5, 30, and 60 sec reaction time before ammonia treatment.

4.1.4. The pH of Au^{3+} solution influence on gold structures

Generally, highly acidic condition (pH 0) of Au^{3+} solution was prepared by dissolving Au metal with aqua regia. At neutral (pH 7) and alkaline (pH 14) conditions were tuned by adjusting with NaOH. The pH effects of Au^{3+} solution on galvanic replacement reaction were depicted in Figure 4.12. The optical property changed from silver to dark brown, light brown and muddy silver when increasing NaOH. The effects of pH on gold structures transformation were confirmed by SEM micrographs. SEM micrographs showed the complexity of the galvanized silver surface was decreased when increasing pH of Au^{3+} at the acidic to alkaline conditions. SEM micrographs of galvanized silver surface indicated the normal condition of galvanic replacement reaction after ammonia treatment. Gold prefer to grow on silver surface as a CLGNs with plate thickness of 80-100 nm. At neutral condition of Au^{3+}, Zen stone-liked gold microstructures with diameter of 10-12 µm was developed as vertical direction. When the pH of Au^{3+} solution was adjusted to alkaline condition (pH 14), the AgCl precipitates was appeared due to insignificant change on galvanized silver surface (Figure 4.12 C).

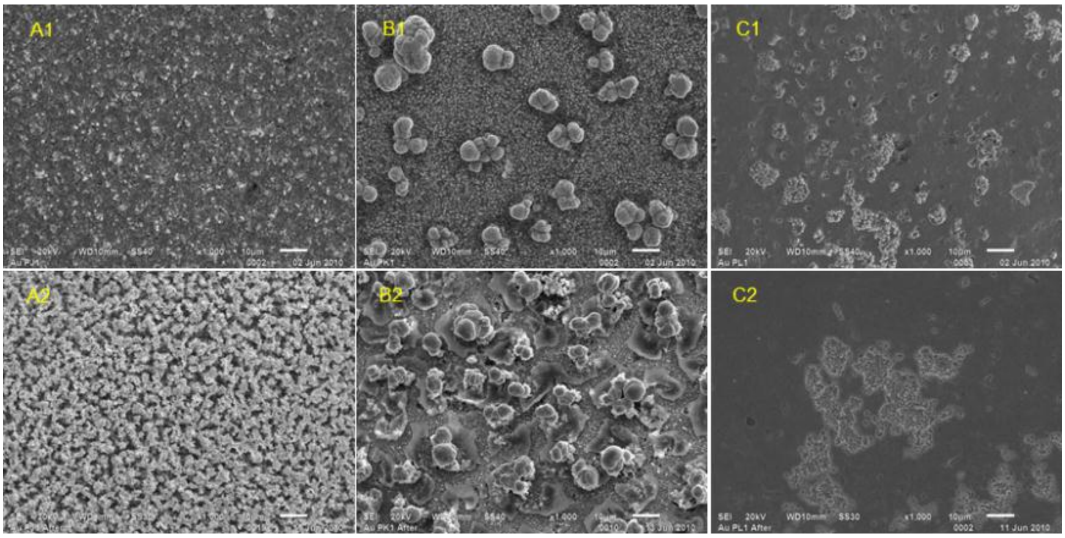

Figure 4.12 Structural developments of coral-liked, Zen stone-liked gold nanostructures, and gold thin film due to pH of Au^{3+} solution with 30 min reaction time. (A, B, and C) SEM micrographs of galvanized silver surface of 5,000 ppm of Au^{3+} solution with pH 0, 7, and 14, reaction time 30 min respectively. (1and 2) SEM micrographs were compared after ammonia treatment.

To observe the elemental composition of galvanized layer at vary pH (7, and 14) by EDS was compared with normal condition (pH= 0). Figure 4.12 shows atomic ratios of galvanized layer at pH 0, 7, and 14 (A, B) before and after ammonia treatment. Atomic ratios of Ag/Au and Cl/Au had good results of 2.33 and 1.43 at pH 0 of Au^{3+} solution. When the pH of Au^{3+} was increased up to neutral, atomic ratios of Ag/Au and Cl/Au was insignificantly decreased to 1.49 and 1.21 although the Zen stone-liked gold microstructures completely changed. However the galvanic replacement reaction Au^{3+} at alkaline condition with Ag metal, atomic ratios of Ag/Au and Cl/Au is more than previous conditions. After ammonia treatment, atomic ratio of Ag/Au was upturn to 108.3 while atomic ratios of Cl/Au dropping to 0.58. However atomic ratios of Ag/Au and Cl/Au at neutral condition are similar to that of acidic condition after ammonia treatment. The EDS mapping of Zen stone-liked gold microstructures clearly indicated in Figure 4.13.

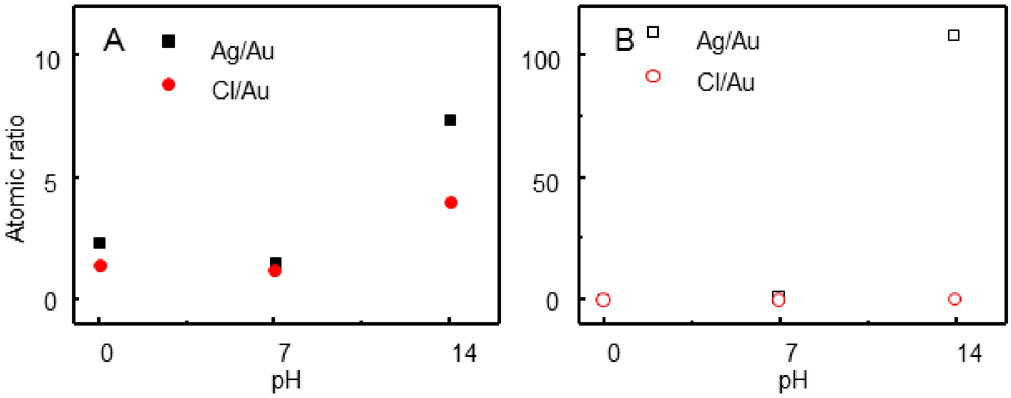

Figure 4.13 Atomic ratios of Ag/Au and Cl/Au on galvanized-layer at pH 0, 7, and 14 (A, B) before and after ammonia treatment.

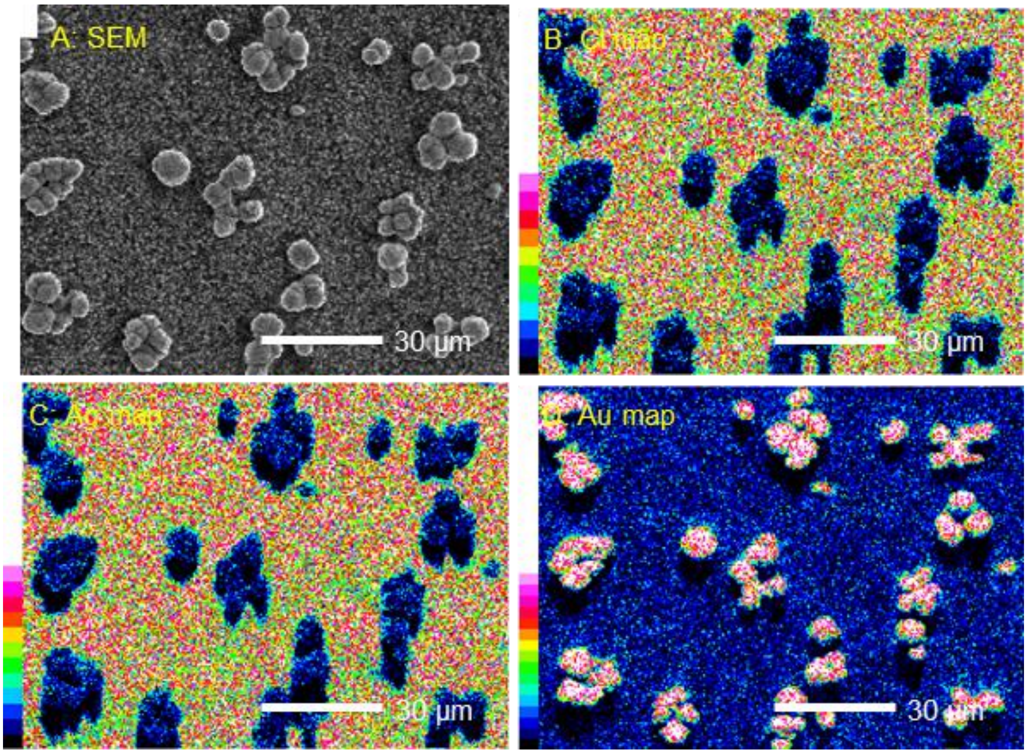

Figure 4.14 EDS mapping of elemental Zen stone liked-gold microstructures (A) SEM micrograph, (B, C, and D) Cl, Ag, and Au mapping.

4.2. Synthesis of NLGNs

Figure 4.14 shows NLGNs using the same chemical as that of CLGNs synthesis. Low magnification SEM micrographs of the complete galvanized layer before and after ammonia treatment are shown in Figure 4.14 (A, B), it is noticeable that the structural changing on the top surface of NLGNs was not observed. Unchangeable NLGNs was implied that the needle structures completely coverage AgCl. The cross-section view of SEM micrographs with back scattering detector was shown in Figure 4.14 (C, D). A white and brown area refers to Au and AgCl that showing NLGNs grew through AgCl structures. Figure 4.14 (E) corresponds to the previous Figure captured with secondary electron detector (SEI) as normal SEM micrographs.

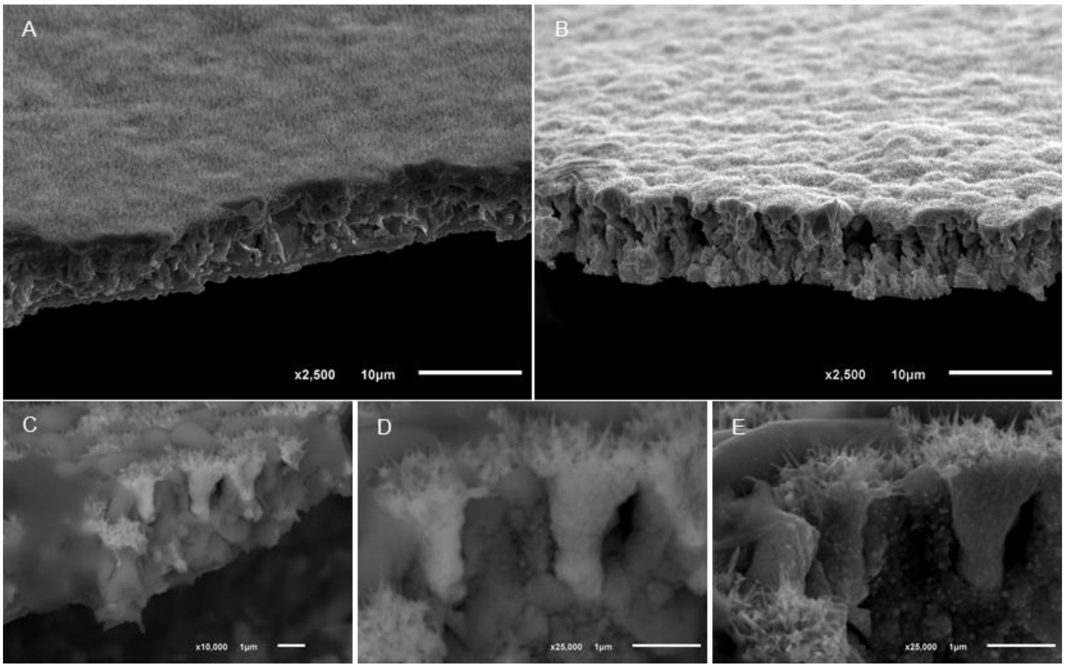

Figure 4.15 (A, B) SEM micrographs of NLGNs before and ammonia treatment (C, D) SEM micrographs with back scattering detector (E) corresponding SEM micrograph with (D).

4.2.1. The effect of NaCl on NLGNs

The NLGNs with single tip was growing with the same condition as that of CLGNs. Silver metal was dipped into 5,000 ppm Au^{3+} with 2 M NaCl, the

NLGNs occurred. Cl^- is key factor of NLGNs growth. When 5,000 ppm Au^{3+} mixed with 2 M NaCl, light yellow no change while silver globules performing the slow change of color to black when galvanic replacement occurred. The different NaCl concentrations (0 M, 0.1M, 0.5 M, 1M, 2M, 4M NaCl) mixing with 5,000 ppm Au^{3+} was monitored at 30 min reaction time as shown in Figure 4.15. The galvanic replacement reaction without adding NaCl, CLGNs was obtained. At 0.1 M NaCl mixing with 5,000 ppm Au^{3+}, thorn-liked gold nanostructures with diameter of 100-500 nm and the length of 1-2 µm was developed blending with AgCl as smooth surface. These structures distinctly noticed after removing AgCl. Larger diameter and the length of thorn-liked gold nanostructures developed over AgCl structure when increasing to 0.3 M NaCl. At the same condition of initial state of NLGNs with tips diameter of 80-120 nm and needle length of 1-1.3 µm joined with thorn-liked gold nanostructures. At the concentration of NaCl was increased to 0.5M, the NLGNs with smaller tip grew longer into vertical direction. Only NLGNs developed on the gold film when increasing NaCl until 3 M NaCl. However, connecting NLGNs layer was not completely covered the total area of silver sacrificed surface.

4.2.2. Micro-channel on AgCl layer

In previous experiment, ammonia treatment was applied for detecting structural transformations of galvanized layer including Au/AgCl composites and Au structures without AgCl precipitates. In this experiment, the ammonia treatment was used to study the middle AgCl layer, 0.5 % w/v NH_3 softly dissolved AgCl on the surface galvanized layer for 15 min. All NLGNs were synthesized using 5,000 ppm Au^{3+} with 2 M NaCl as 30 min of galvanic replacement reaction. Figure 4.17, SEM micrographs show galvanized surface which was removed AgCl at 0, 0.5, and 10 % w/v NH_3. Micro channel with diameter of 300-500 nm was detected on AgCl surface, original NLGNs was fabricated as shown in Figure 4.17 A. When using low concentration of NH_3, AgCl was not completely removed. The residue of AgCl layer showed in Figure 4.17 (B), the micro channels only occurred on AgCl layer. This phenomenon was confirmed that the gold surface insignificant detected micro channel. However AgCl was completely dissolved by using 10 % w/v which the micro channel cannot observe.

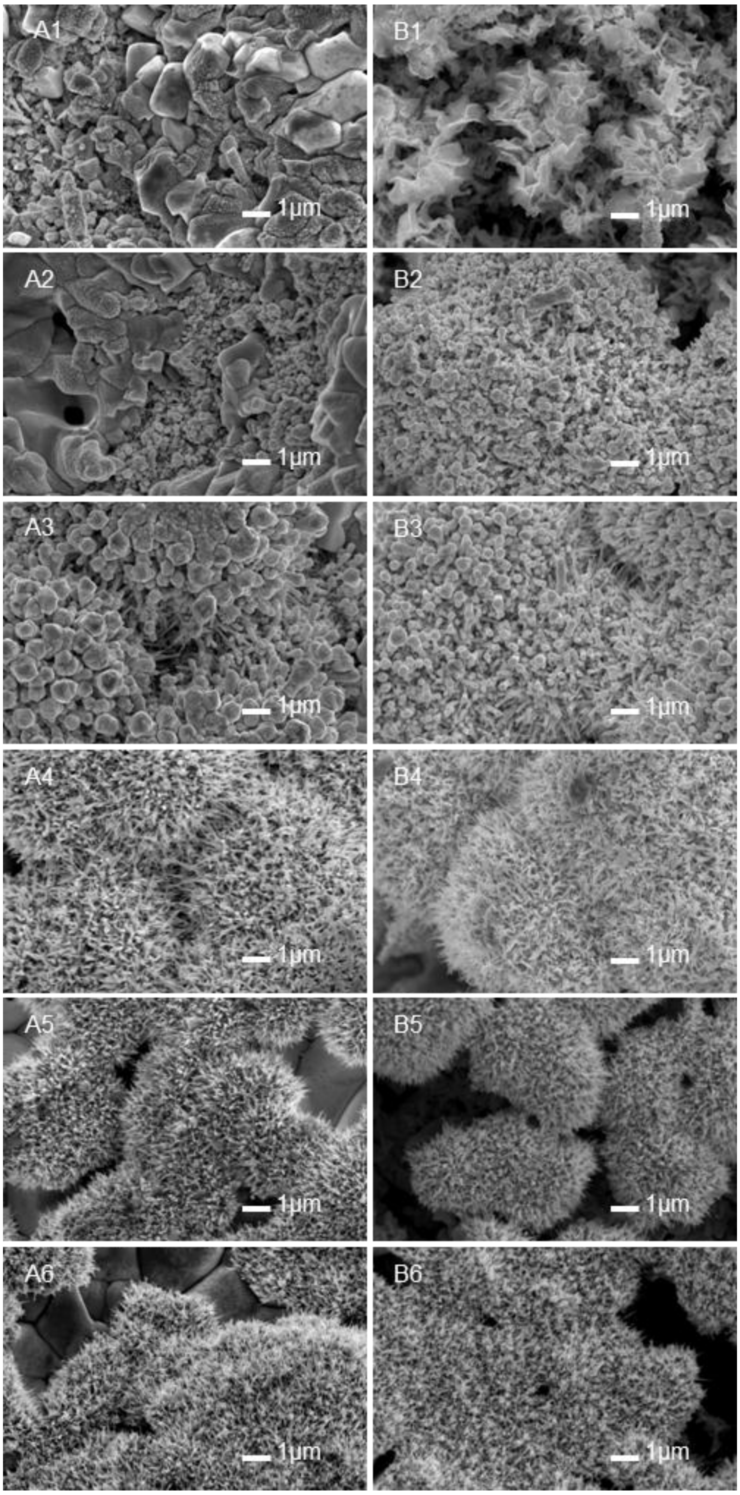

Figure 4.16 (A1-A6) Structural developments of NLGNs by galvanic replacement reaction, silver globules and 5,000 ppm of Au^{3+} solution was mixed 0, 0.1, 0.3, 0.5, 1, 2 M NaCl at 30 min respectively. (A2-A6) structure developments of NLGNs after remove AgCl by ammonia treatment.

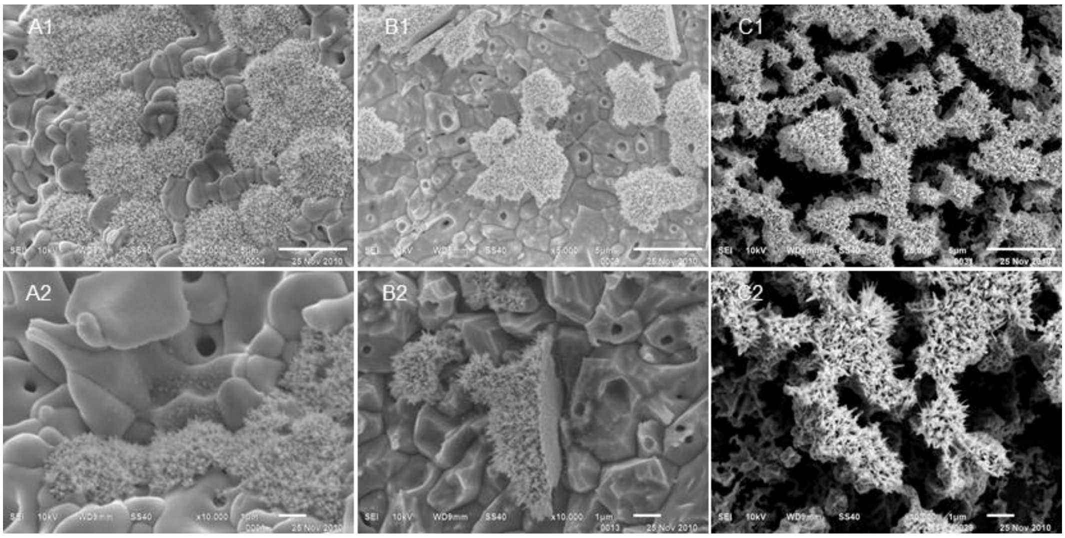

Figure 4.17 (A, B, and C) SEM micrographs of galvanized silver was removed AgCl with 0, 0.5, and 10 % w/v NH_3. (1 and 2) SEM magnifications take with 5,000x and 10,000x

4.2.3. Time dependent evolution of NLGNs

Structural evolution of NLGNs due to reaction time of galvanic replacement reaction was monitored by SEM. From Figures 4.17, SEM micrographs of galvanized layer were observed the growth mechanism steps of NLGNs by monitoring the reaction time as follows: 0, 5, 10, 20, and 30 min. Figure 4.17 A1, SEM micrographs of silver sacrificed surface before galvanic replacement reaction has taken place with insignificant changed after ammonia treatment. After 5 min galvanic replacement reaction, AgCl concomitant with domain size of 1-1.5 µm grew over gold structures. The micro porous gold with domain size of 1-1.5 µm was observed after removing AgCl. The differential structures comparable to similarly condition of CLGNs, the plate-liked gold nanostructures cannot develop on gold film at 5 min reaction time. When the reaction time increased to 10 min (Figure 4.17 A3), gold cluster with domain size of 5-6 µm were generated through AgCl layer. Little plate-liked gold nanostructures were developed on the gold cluster and no AgCl feature co-deposited on gold cluster. Continuous galvanic replacement reaction occurred as the reaction time increased to 20 min (Figure 4.14 A4). Selective deposition of gold due to galvanic reaction was filled on gold cluster, little plate-liked gold nanostructures transformed to NLGNs.

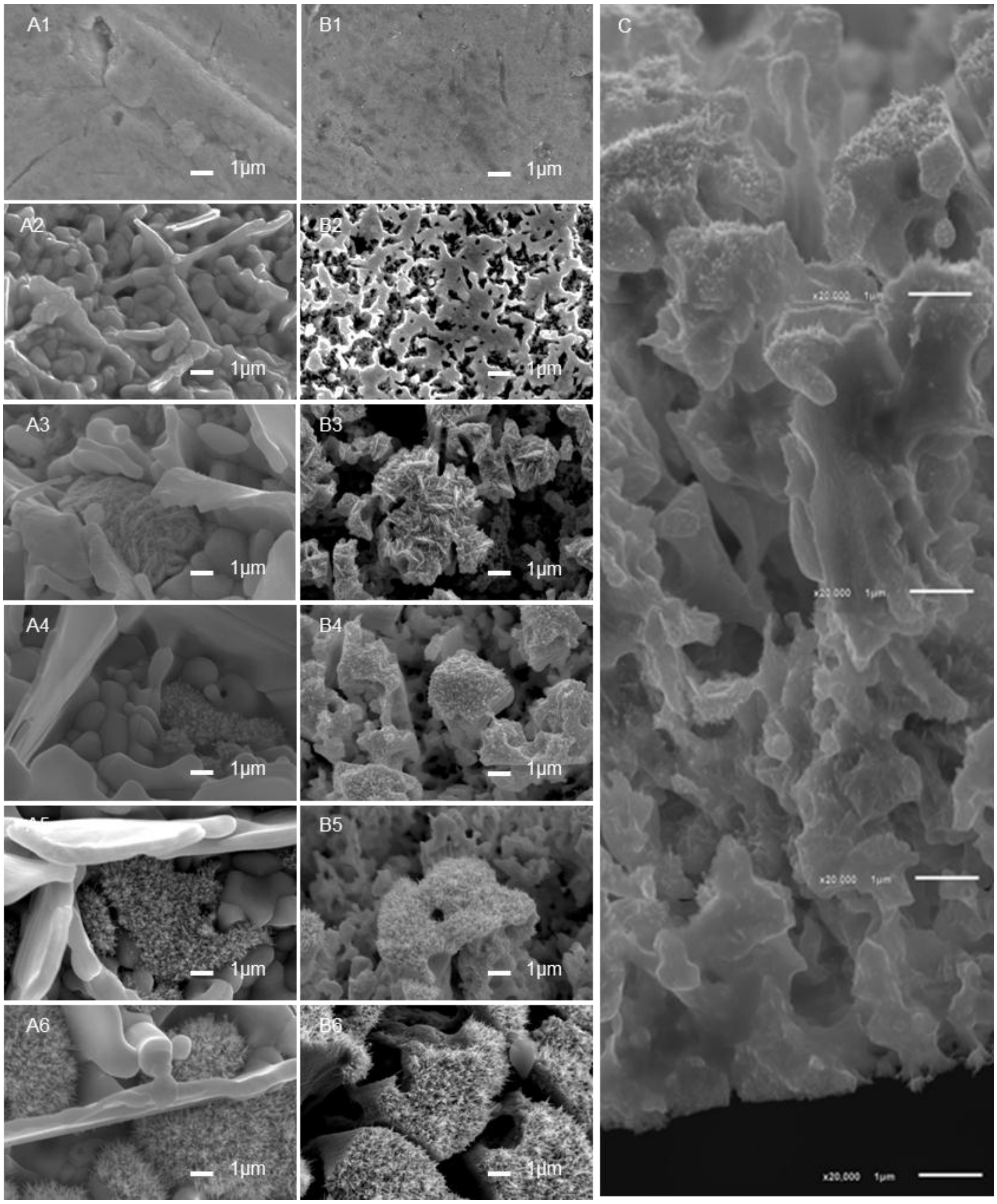

Figure 4.18 (A1-A6) Time dependent of NLGNs by galvanic replacement reaction between silver globules and 5,000 ppm Au^{3+} was mixed 2 M NaCl at 0, 5, 10, 20, 30 and 60 min respectively. (A2-A6) corresponding of NLGNs after removing AgCl by ammonia treatment.

When the reaction time increased to 30 and 60 min (Figure 4.14 A5, A6), finally NLGNs was generated on gold cluster. The vertical panorama SEM micrograph shows the detail growth of NLGNs. Cross section vertical panorama SEM micrograph with thinness of 13-15 µm on NLGNs was captured at 30 min reaction time. The galvanized layer at initial state, dense gold was epitaxial depositing with continuous layer.

4.2.4. X-ray diffraction (XRD) pattern of the CLGNs and NLGNs

Figure 4.20 shows X-ray diffraction (XRD) pattern of the CLGNs and NLGNs after ammonia treatment. The XRD pattern obtained four peaks at 38.12, 44.12, 64.48, 77.5 corresponding to the (111), (200), (220), (311) planes of a face centered cubic lattice [17, 18]. It is worth noting that the intensity ratio (coral 0.42), needle 0.37) of the 200 to 111 that one is lower than the conventional intensity ratio (gold powder 0.52) [19, 20]. These observations imply that the deposited of CLGNs and NLGNS tend to nucleate and grow into their surfaces terminated by the lowest energy (111) facets

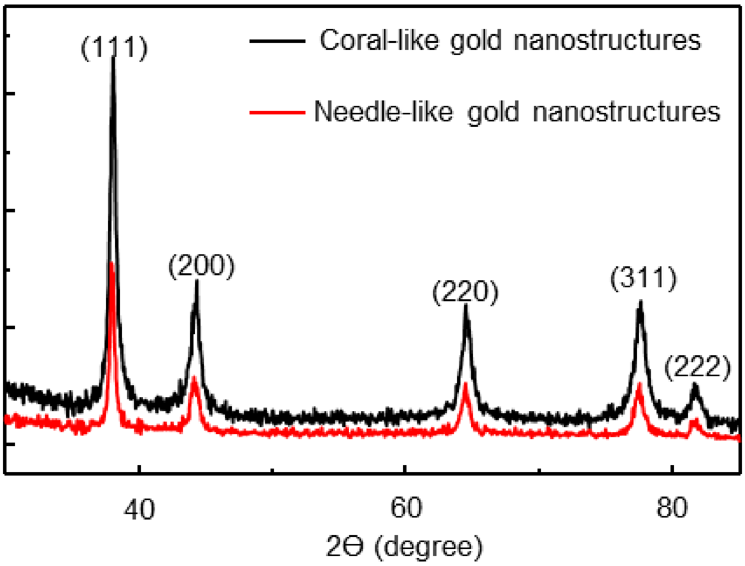

Figure 4.19 XRD patterns of CLGNs and NLGNs after ammonia treatment

4.3. Synthesis of standing coral-liked gold nanoporous

The standing CLGPs synthesis by using ultrasonic assisted. (1) The advantage of the method, fast galvanic creation complex nanostructures, (2) no additive agent such as capping agent, stabilizer, reducing agent, and (3) easy cleaning. Fabrication of CLGPs as microstructures using ultrasonic radiation was assisted at room condition.

4.3.1. Optical property of Au/AgCl composites

Figure 4.22 shows digital image as a video snap shot of galvanic reaction (A) 5,000 ppm of Au^{3+} before galvanic replacement reaction, (B-E) galvanic replacement reaction at 00:00.000, 00:0.083, 00:09.167, 00:20.242, and 07:13.917 reaction time (sec). The fast galvanic replacement reaction created Au/AgCl composites at 0.83 sec, the color of silver surface change to black (Figure 4.22 (B compares with C)). Au/AgCl composites were ejected from silver surface when the reactions continuously occurred to 9.16 sec. the clearly phenomena was observed at 20 sec, the black diffused to Au^{3+} solution while silver color appeared on silver surface. Au/AgCl composites were released under ultrasonic radiation condition due to regenerate Ag free surface. Regenerative free Ag surface and galvanic replacement reaction occurred as circle galvanic replacement reaction and completely consumed Ag sacrifice at 7-10 min.

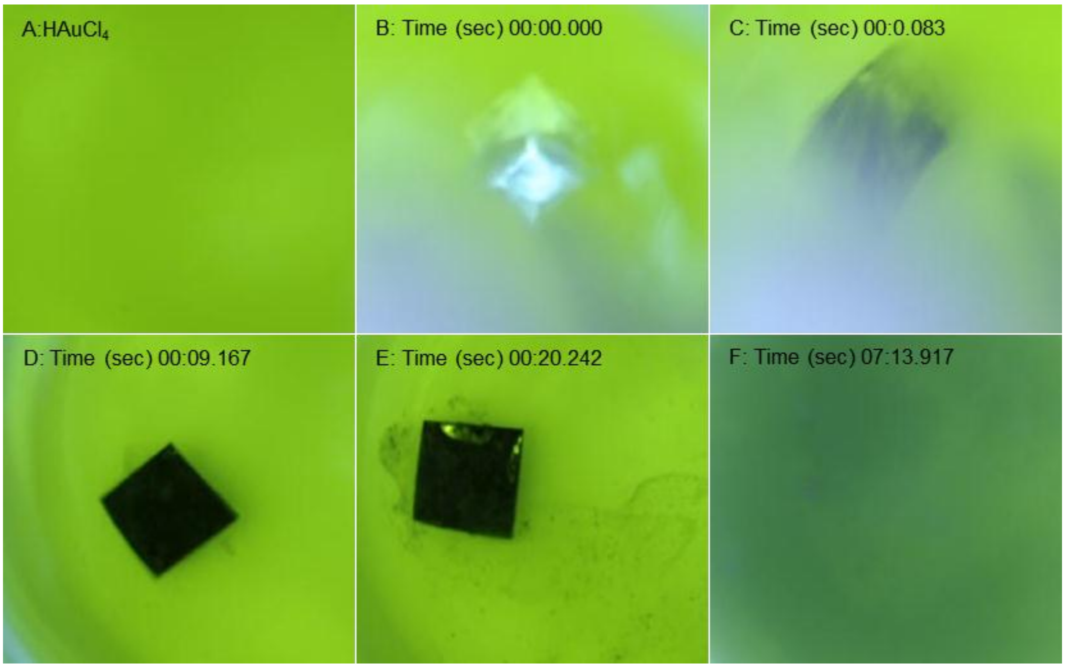

Figure 4.20 Digital images of snap shot video of galvanic reaction (A) 5,000 ppm Au^{3+} before galvanic replacement reaction (B-E) galvanic replacement reaction at 00:00.000, 00:0.083, 00:09.167, 00:20.242, and 07:13.917 reaction time (sec).

4.3.2. UV-visible change of Au^{3+} solution on galvanic replacement reaction

Optical absorption of Au^{3+} before and after galvanic replacement reaction was investigated by UV-visible spectroscopy. The Figure 4.23 shows UV–visible absorption spectra of aqueous Au^{3+} solution before and after galvanic replacement reaction. The strong adsorption band at 220 nm and shoulder at 290 nm were decreased when galvanic replacement reaction completely consumed Ag. The orange-yellow color of the gold (III) ion solution was insignificantly changed to green after galvanic replacement reaction. Figure 4.23 (A, B) inset image shows the color of Au3+ solution before and after galvanic reaction.

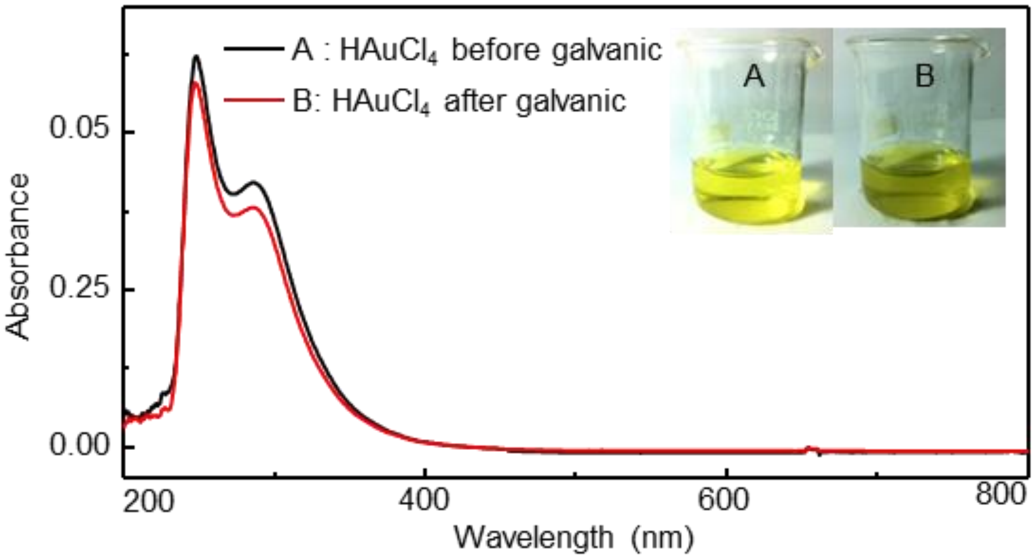

Figure 4.21 (A, B) UV-visible spectra of 5,000 ppm Au^{3+} diluted to 10 ppm before and after galvanic replacement reaction. Image inset: Digital image of Au^{3+} solution.

4.3.3. The morphology of CLGPs

SEM micrographs of Au/AgCl composites and CLGPs after removing AgCl show in Figure 4.24. Au/AgCl composites with domain size of 80-300 nm at upper layer was formed Au/AgCl micro plates with a thinness of 1-2 µm. A continuous layer of AgCl part with domain size of 0.3-1 µm was investigated lower of Au/AgCl composites. CLGPs were generated when AgCl was removed under NH_3 condition. Pore size of CLGPs was the combination of between nano and micropores. Pore size of micropores about 150-300 nm was produced on the surface of CLGPs and pore size of nanopore about 30-60 nm was investigated inside of micropores. Figure 4.25 shows pore size distribution of CLGPs. Inset Figure 4.25 was the SEM micrograph which was captured at high magnification (100,000X) of CLGPs.

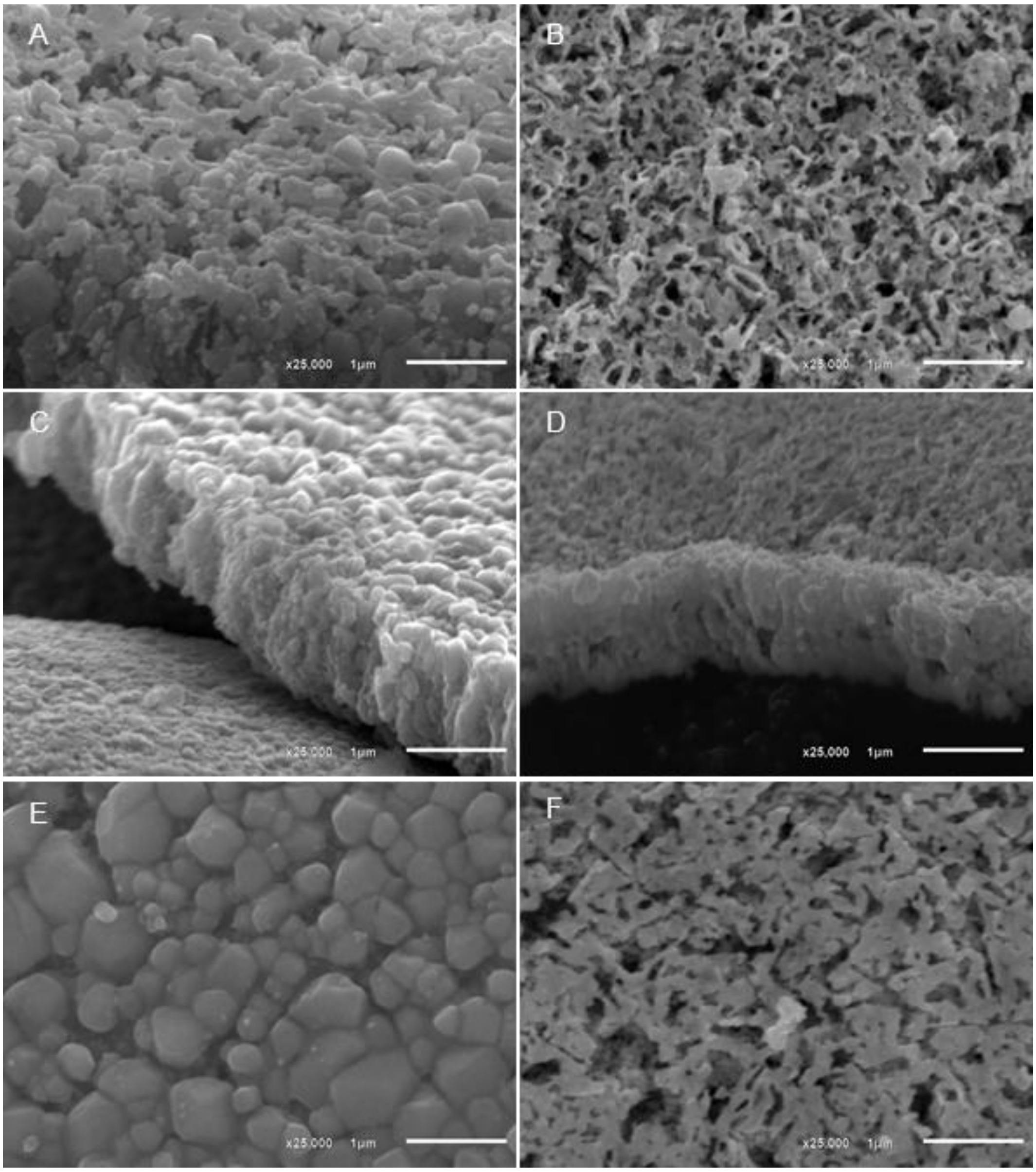

Figure 4.22 CLGPs synthesis by using ultrasonic assisted, (A, C, and E) SEM micrographs CLGPs before ammonia treatment and (B, D, and F) after galvanic replacement reaction.

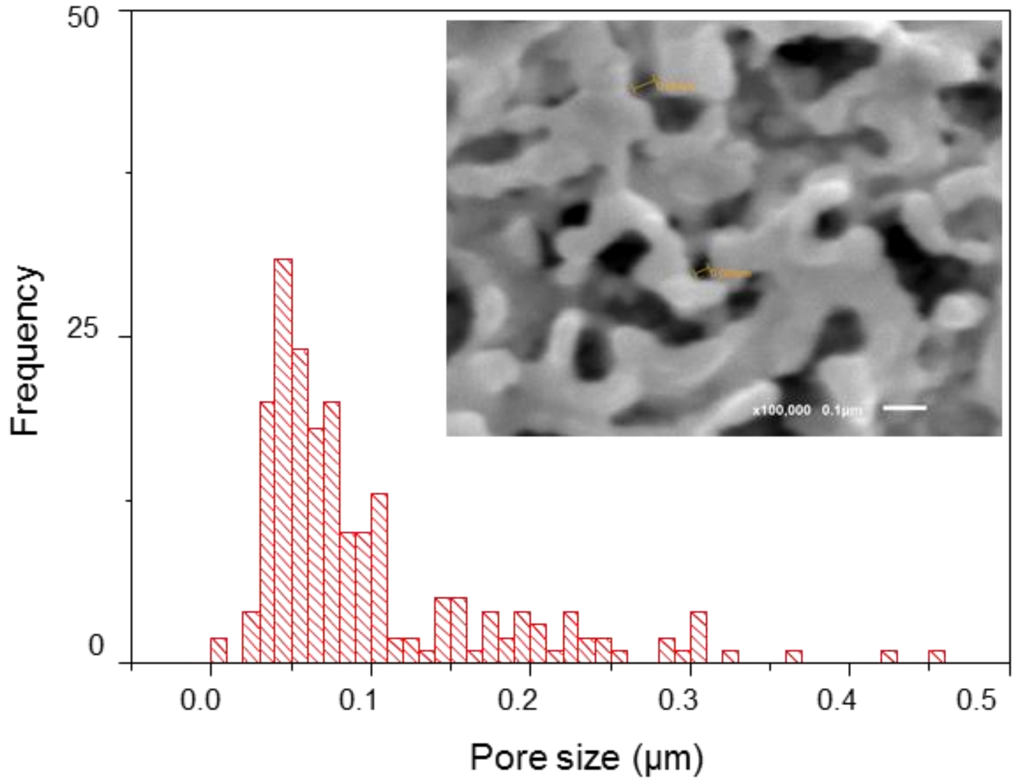

Figure 4.23 Pore size distribution of CLGPs show combinations of micro and nanoporous on structures, (inset) SEM micrograph captured with high resolution.

4.3.4. Elemental composition of Au/AgCl composites and CLGPs

The elemental composition of Au/AgCl composites and CLGPs were shown in Figure 4.25. EDS spectrum showed high intensity of Au, Ag, and Cl at 2.21, 2.621, and 2.983 keV, the atomic ratio of Au/Ag/Cl is about 19.86, 44.96, 35.17. After removing AgCl by ammonia treatment, atomic ratio of Au was strongly increased to 96.27 while Ag and Cl about 3.74 and 0 were detected. The morphology of CLGPs included Ag inside gold structure.

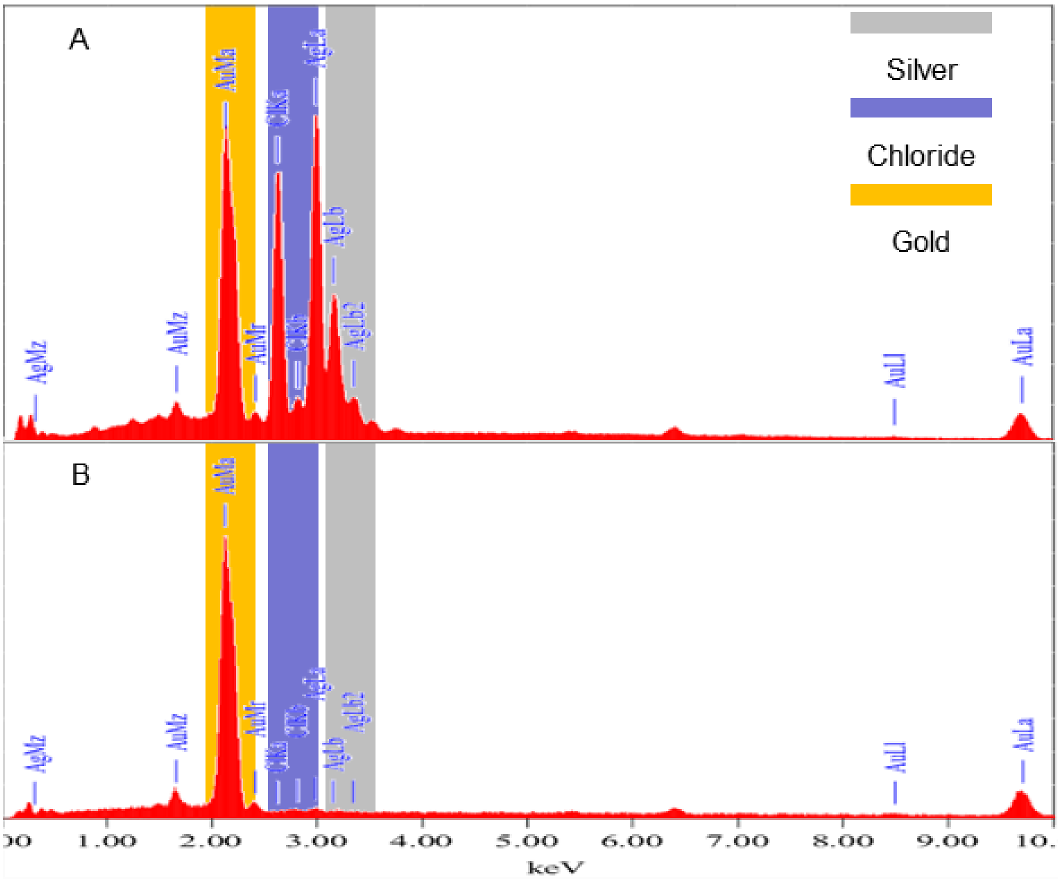

Figure 4.24 EDS spectra of Au/AgCl composites and CLGPs

4.3.5. Proposed circle galvanic replacement reaction mechanism.

Schematic diagram of circle galvanic replacement reaction showed in Figure 4.25. The film is automatically detached from the sacrificed silver plate as the film becomes thicker under ultrasonic radiation. The mechanism of circle galvanic replacement reaction could be explained auto ejection of the Au/AgCl composites: (A) original of a clean Ag metal before immersed to Au^{3+} solution, non-galvanic replacement reaction, (B) while clean Ag metal was dipped into Au^{3+} solution, Rapid epitaxial growth of Au film on the clean Ag surface, (C) precipitation and formation of AgCl precipitates was formed on Au film and, (D) Au/AgCl nanocomposites when prolong galvanic reaction, (E) AgCl underlay start development under Au/AgCl nanocomposites, (F) ultrasonic assisted detachment of the (galvanic generated) interpenetrated Au/AgCl nanocomposites film with AgCl underlay from the silver plate.

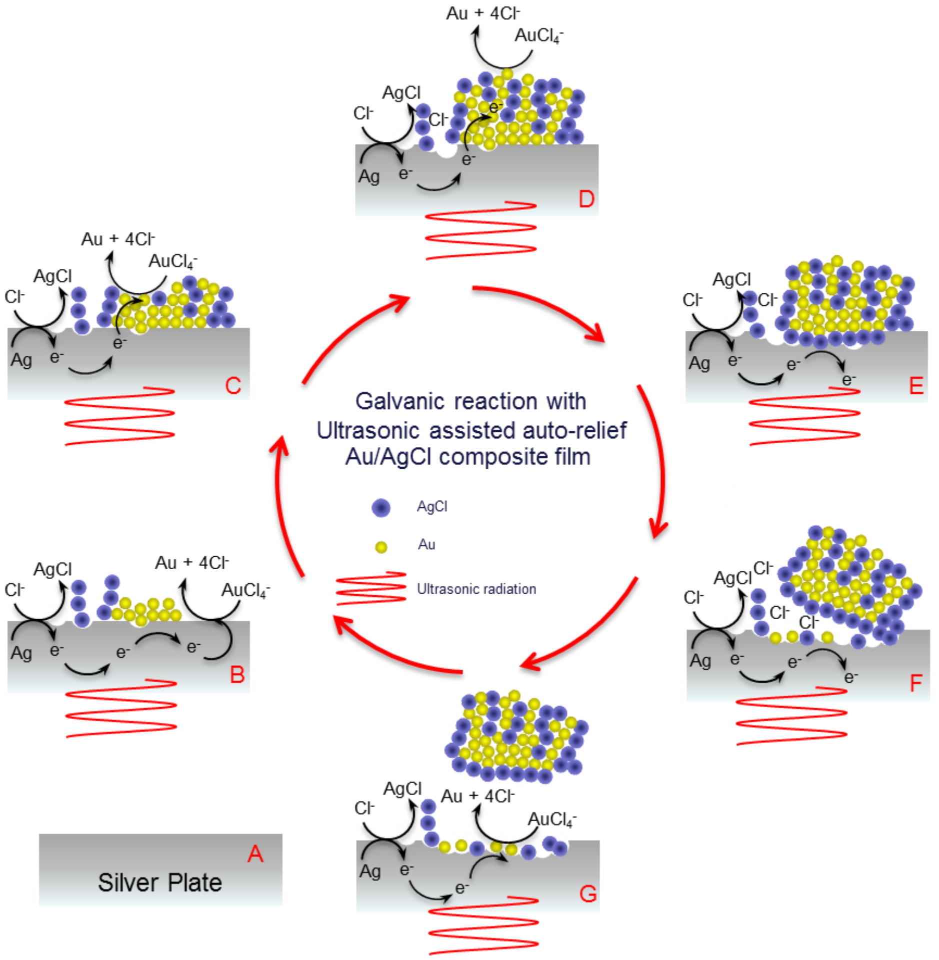

Figure 4.25 Schematic diagram of circle galvanic replacement reaction show the film is automatically detached from the sacrificed silver plate, *i.e.*, as the film becomes thicker. The mechanism of the nanoporous gold film development included: (A) supply/regeneration of a clean Ag surface (B) rapid epitaxial growth of Au film on the clean Ag surface (C) precipitation and formation of AgCl precipitates on Au film (D) formation of interpenetrated Au/AgCl nanocomposite (E) development of AgCl underlay (F) ultrasonic assisted detachment of the (galvanic generated) interpenetrated Au/AgCl nanocomposite film with AgCl underlay from the silver plate. The detachment occurs at the interface between Ag plate and the AgCl underlay. The ultrasonic assisted auto-detachment enables a self-initiated formation of clean Ag surface of the silver plate.

4.3.6. Surface enhanced Raman scattering (SERS) activity of CLGPs

The SERS studies were done by using a DXR Raman microscope. The SL crystals were transferred to a thin glass plate, washed with ethanol, and dried under ambient conditions. The SERS measurements were using crystal violet (CV) and rhodamine 6G (R6G) as the Raman probe molecule. The various concentrations of CV and R6G solutions were prepared in water at (10^{-3}-10^{-6}M). The 1 µL of standing CLGPs were dropped in glass slide and dried under vacuum condition. After that the 1 µL required concentration of R6G and CV were dropped on standing CLGPs and dried under vacuum condition. Figure 4.8 and 4.9 show the SERS spectra of R6G and CV collected from the surface standing CLGPs using 532 nm excitation lasers with 1s acquisition time. All the peaks of R 6G and CV have been assigned in Table 1 and 2.

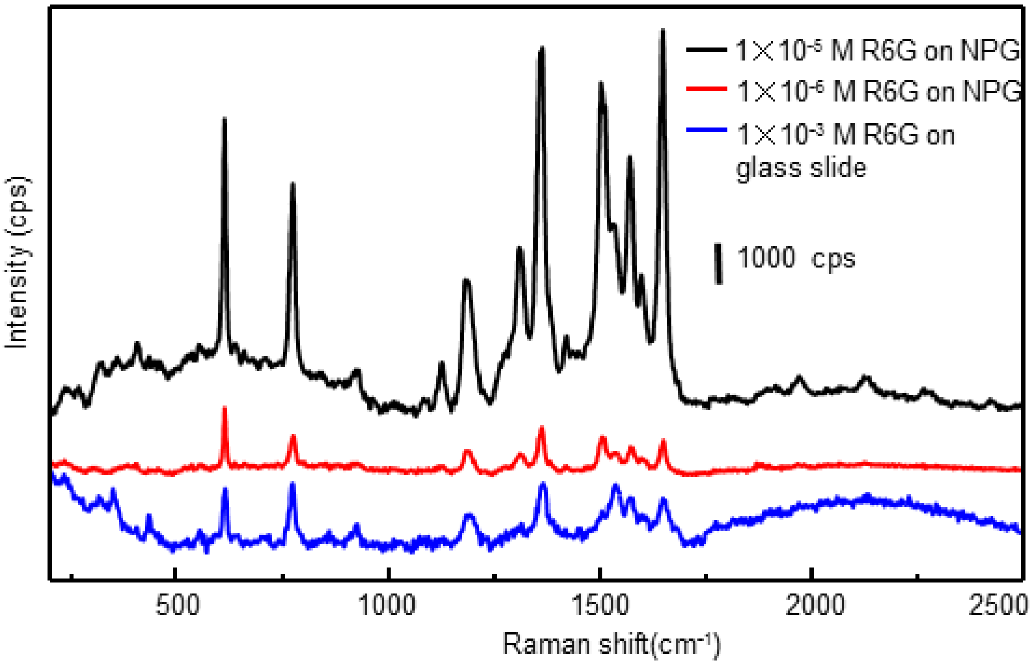

Figure 4.26 SERS of $1x10^{-5}$ and $1x10^{-6}$ M R6G on CLNPs compared with $1x10^{-3}$ M R6G on glass slide.

Table4.1. Assignment of Raman bands of the SERS spectrum of R6G [72]

Raman band assignment	Raman shift (cm^{-1})
Xanthenes ring stretching, in plane C-H bending	1647
Xanthenes ring stretching, in plane N-H bending	1571
Xanthenes ring stretching, C-N stretching, C-H bending, N-H bending	1508
Xanthenes ring stretching, in plane C-H bending	1360
In plane xanthenes ring breathing	
N-H bending, CH_2 waggling	1309
In plane xanthenes ring deformation, C-H bending, N-H bending	1181
Out of plane C-H bending	770

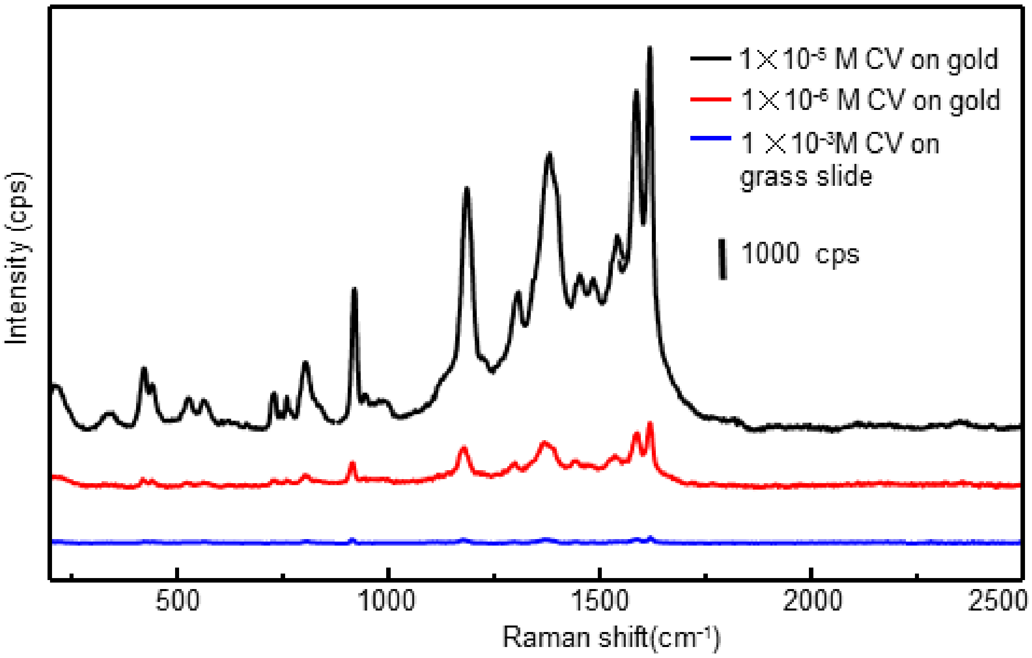

Figure 4.27 SERS of 1x10^{-5} and 1x10^{-6} M CV on CLNPs compared with 1x10^{-3} M R6G on glass slide

Table4.2. Assignment of Raman bands of the SERS spectrum of CV [73]

Raman band assignment	Raman shift (cm^{-1})
ring C-C stretching	1627
ring C-C stretching	1592
ring C-C stretching	1542
+ ring deformation	1484
ring C-C stretching	1450
N-phenyl stretching	1379
ring C-C stretching	1305
ring C-H bend (II)	1186
ring C-H bend (II)	1131
ring skeletal vib. of radical orientation	992
ring skeletal vib. of radical orientation	922
ring C-H bend (⊥)	819
ring C-H bend (⊥)	768
ring C-H bend (⊥)	738
ring skeletal vib. of radi cal orientation	633
ring skeletal vib. of radi cal orientation	572
ring skeletal vib. of radi cal orientation	538
Ph-C+-Ph bend(⊥)	432
Ph-C+-Ph bend(II)	348
Breathing of central bonds	232
(II) and (⊥) means in-plane and out-of-plane, respectively	